Hindawi
Shock and Vibration
Volume 2021, Article ID 9695139, 13 pages
https://doi.org/10.1155/2021/9695139

Research Article

Modeling Research and Test Verification of the Seismic Response of a Multistage Series Liquid Tank

Xiaoguang Yao, Lijun Meng, Peng Chu, and Liang Yao

School of Mechanical Engineering, Xijing University, Xi'an 710123, China

Correspondence should be addressed to Xiaoguang Yao; xgyao_1980@sina.com

Received 11 August 2021; Accepted 29 October 2021; Published 17 November 2021

Academic Editor: Honghao Li

Liquid storage tanks are lifeline structures and strategically very important. Heavy damages or even collapse of these facilities subjected to strong earthquakes may cause disastrous consequences. In this paper, the seismic response of a multistage series liquid storage tank was simulated by a finite element method and verified by a scaled-down experiment. The structural flexibility of the tank and the liquid-structure coupling characteristics between the liquid and tank wall were considered in the research. A multimass-block and spring model was employed to be equivalent to the longitudinal vibration of the liquid in the storage tank. The relationships between the connection springs and the elements of the stiffness matrix were explicitly deduced. The seismic response analysis of a four-stage series liquid tank was carried out, and the acceleration response, the stress response of the tank, and the vertical vibration of the liquid were obtained. The experimental results are in good agreement with the simulation results, which verifies the effectiveness of the modeling method in this paper.

1. Introduction

Liquid storage tanks are lifeline structures and strategically very important since they have vital use in industries and nuclear power plants [1]. Heavy damages or even collapse of these facilities subjected to strong earthquakes may cause disastrous consequences such as explosions, fires, and environmental contaminations [2]. The seismic safety performance of a large liquid storage tank is crucial and has a direct effect on the economic performance, reliability, and service life of the tank [3]. Analytical solutions for the seismic fluid-structure interaction of tanks are used by analysts and engineers for a number of purposes, including preliminary sizing, risk assessment, and verification of numerical models [4].

The seismic behavior of the liquid storage tank is highly complex due to liquid-structure interaction, leading to a tedious design procedure from an earthquake-resistant design point of view. To improve the structural seismic response of the liquid storage tank, in the past few decades, scholars have proposed many effective research methods including the concentrated mass method, the distributed mass method, and the test analysis method. Housner [5] and Rosenblueth and Newmark [6] developed a lumped mass model of rigid liquid storage tanks and investigated its seismic response. These models were modified by Haroun [7], which takes into account the flexibility of the tank wall in the seismic analysis. In the concentrated mass method, the contained liquid is considered as incompressible and inviscid and has irrotational flow. The typical models include the single-degree-of-freedom model [8], two-degree-of-freedom model [9–11], and three-degree-of-freedom model [12–18]. In [8], a simplified one-degree-of-freedom idealization was set up and particular attention was paid to the sloshing effects. In the two-degree-of-freedom model, as described in [9–11], the liquid mass was considered as a convective mass which caused the sloshing phenomenon and an impulsive mass which accelerated along with the tank. In the three-degree-of-freedom lumped mass model, the entire tank liquid mass vibrates in three distinct patterns: sloshing mass, impulsive mass, and rigid mass.

In the research using the distributed mass model [19–27], the finite element method is generally used to establish the model of the liquid storage tank for liquid-structure coupling

analysis. The tank wall is always regarded as the structure element, and the liquid is regarded as the fluid element. According to the relative motion relationship between the tank and the liquid, the motion coordination constraints of the structure element and fluid element are established. Then, the seismic excitation is applied to analyze the dynamics of the tank and fluid. Aiming at calculating sloshing frequencies, as well as sloshing transient response under horizontal seismic excitation, Karamanos [20, 21] presented a finite element formulation for earthquake-induced sloshing in horizontal-cylindrical industrial vessels. Jingyuan Li [23] adopted the finite element software ABAQUS to trace the dynamic response history of a large reinforced concrete storage tank during different seismic excitations. The dynamic characteristics and failure modes of the tank's structure were investigated by considering the rebar's effect. Aruna Rawat [24, 25] investigated the three-dimensional ground-supported cylindrical and rectangular rigid liquid storage tanks filled with water and subjected to seismic base excitation. The analyses of the tanks were carried out using coupled acoustic-structural and coupled Eulerian–Lagrangian approaches of the finite element method. In [26], the numerical seismic response of liquid storage tanks isolated by bilinear hysteretic bearing elements was investigated under long-period ground motions. Finite shell elements for the tank structure and boundary elements for the liquid region were employed. Fluid-structure equations of motion were coupled with the governing equation of the base-isolation system to represent the whole system behavior. In [27], numerical analyses were performed by means of a detailed finite element model, considering the exact geometry of the elevated steel tank structure and the fluid-structure interaction effects for an arbitrary level of fluid filling, as well as the nonlinearities introduced by the various bracing systems.

In the research using the test analysis method [28–30], a real or scaled model of the liquid tank is generally processed, and the test research is carried out by using the earthquake occurrence test bed. In [28], a series of forced vibration tests, whose measured response was considered as a benchmark, were carried out on a cylindrical tank experimental model. All of the test parameters were scaled according to similitude laws. Jang Ho Park [29] presented dynamic test results of a cylindrical liquid storage tank under horizontal earthquake excitation to investigate its dynamic behavior characteristics, including beam-type and oval-type vibrations. Bae and Ho Park [30] presented the results of shaking table tests performed to examine the dynamic behavior of a scaled cylindrical steel tank model considering the presence or absence of a fixed roof and added mass at the top of the tank for various fluid levels.

At present, there are many studies about the seismic response analysis of a single tank; however, research on the analysis of a multistage series tank is not deep enough. Different from the single-stage tank, the multistage series tank is tall, and the slenderness ratio is relatively large. Therefore, the structural flexibility of the tank needs to be considered. The "forced vibration" effect caused by the liquid-structure interaction should also be considered. In addition, the research literature mostly considers only the lateral sloshing effect of the liquid, and the longitudinal vibration characteristic is ignored. Aiming at the seismic response analysis of the multistage series liquid storage tank, this paper constructed a finite element model including the liquid-structure coupling effect of the tank wall and liquid, as well as the longitudinal vibration characteristic of the liquid. The research on the modeling method and experimental verification were simultaneously carried out in this paper.

2. Mass Matrix and Longitudinal Stiffness Matrix

2.1. Mass Matrix. Due to the structural flexibility and the coupling effect, the multistage series tank will form a tower effect when it encounters an earthquake; that is, the ground excitations will be multiplied on the tank. The important feature of the liquid-structure coupling problem is the interaction of the two-phase medium. The solid structure will deform or move under the action of the fluid load, and this deformation or movement will in turn affect the amplitude and distribution of the fluid load. In this investigation, the liquid is considered incompressible and inviscid and has irrotational motion. For the quasistatic flow field and linear elastic structure with small deformation, the equation of the displacement-pressure format of the liquid-structure coupling system can be expressed as

$$\begin{bmatrix} \mathbf{M}_s & 0 \\ -\mathbf{Q}^T & \mathbf{M}_f \end{bmatrix} \{\ddot{u}\ \ddot{p}\} + \begin{bmatrix} \mathbf{K}_s & \dfrac{\mathbf{Q}}{\rho_f} \\ 0 & \mathbf{K}_f \end{bmatrix} \begin{Bmatrix} \mathbf{u} \\ \mathbf{p} \end{Bmatrix} = \begin{Bmatrix} \mathbf{F}_s \\ 0 \end{Bmatrix}, \tag{1}$$

where $\boldsymbol{p}$ is the pressure vector of the fluid node; $\boldsymbol{u}$ is the displacement vector of the solid node; $\mathbf{Q}$ is the liquid-structure coupling matrix; $\mathbf{M}_f$ and $\mathbf{K}_f$ are the mass matrix and stiffness matrix of the fluid, respectively; $\mathbf{M}_s$ and $\mathbf{K}_s$ are the mass matrix and stiffness matrix of the structure, respectively; $\mathbf{F}_s$ is the external load vector; and ρ_f is the density of the liquid.

If the influences of fluctuation and compressibility of the liquid are ignored, the dynamics problem of the liquid-filled tank can be simplified as the structural dynamics problem with additional mass. The dynamic equation (1) can be rewritten as

$$\begin{bmatrix} \mathbf{M}_s & 0 \\ -\mathbf{Q}^T & 0 \end{bmatrix} \{\ddot{u}\ \ddot{p}\} + \begin{bmatrix} \mathbf{K}_s & \dfrac{\mathbf{Q}}{\rho_f} \\ 0 & \mathbf{K}_f \end{bmatrix} \begin{Bmatrix} \mathbf{u} \\ \mathbf{p} \end{Bmatrix} = \begin{Bmatrix} \mathbf{F}_s \\ 0 \end{Bmatrix}. \tag{2}$$

Substituting equation (2) into (1) and eliminating vector $\mathbf{p}$, one can obtain

$$(\mathbf{M}_s + \mathbf{M}_s')\ddot{u} + \mathbf{K}_s\mathbf{u} = \mathbf{F}_s, \tag{3}$$

where $\mathbf{M}'_s = \mathbf{Q}\mathbf{K}^{-1}\mathbf{f}\mathbf{Q}^T/\rho_f$ is the additional mass matrix representing the effect of the fluid on the solid structure. The key to the dynamic problem, therefore, lies in the processing of the additional mass matrix.

Since the quality characteristics of the tank structure and liquid are different, the quality of the two is treated separately in the modeling process. When calculating the mass attributes of the tank structure, it is assumed that the structural mass is uniformly distributed. According to the inviscid feature of the liquid, when the storage tank is bent and deformed laterally, most of the liquid will move in parallel with the structure of the tank, except for the liquid near the free surface. Besides, when the tank is deformed longitudinally, the liquid will only follow the movement of the tank bottom, provided that the influence of the longitudinal deformation of the tank on the diameter is ignored. Accordingly, the liquid in the tank is only counted as the translational mass, and the moment of inertia is ignored. The mass matrix of the liquid unit can be written as

$$\mathbf{M}_s^{'e} = \mathbf{M}_f^e = \begin{bmatrix} m_f^e & 0 & 0 & 0 & 0 & 0 \\ & m_f^e & 0 & 0 & 0 & 0 \\ & & m_f^e & 0 & 0 & 0 \\ & \text{symm} & & 0 & 0 & 0 \\ & & & & 0 & 0 \\ & & & & & 0 \end{bmatrix}, \tag{4}$$

where $m_f^e = \int_{V^e} \rho_f \mathrm{d}V_f^e$, in which m_f^e is the mass of the liquid unit and V_f^e is the volume of the liquid unit.

2.2. Longitudinal Stiffness Matrix. In order to simulate the longitudinal vibration characteristics of the multistage series liquid storage tank, a multimass-block model is employed to equivalent the longitudinal vibration of the liquid. Taking the three-mass-block model of a single-stage liquid-filled storage tank as an example, its structure diagram, mechanical model, and calculation model are shown in Figure 1. The liquid in the tank is divided into three mass blocks marked as m_{l1}, m_{l2}, and m_{l3}, respectively. The tank is equivalent to a massless beam, and the mass properties of the tank are assigned to the nodes of the beam elements in the form of concentrated mass. Taking the mass assignment process of a certain section of the tank as an example, as illustrated in Figure 1(a), the mass of the tank wall between nodes a and g is divided into three parts according to its structural characteristic. Then, the mass marked as m_{i-1} between nodes a and c is assigned to node b, and the mass marked as m_i between nodes c and e is assigned to node d. Similarly, the mass marked as m_{i+1} between nodes e and g is assigned to node f. By repeating this, the equivalent process of tank mass to the nodes of the massless beam can be completed.

The position of the storage tank at the free surface of the liquid is marked as 5, as illustrated in Figure 1(c). The positions of centroids of the three liquid mass blocks are marked as 4, 3, and 2, respectively. The connecting part of the tank barrel section and tank bottom is marked as 1. The symbols l_1, l_2, and l_3 represent the liquid heights corresponding to the three mass blocks, respectively. The tank is cylindrical with the inner diameter $2a$, the thickness of the wall is h, the elastic modulus of the material is E, and Poisson's ratio is μ. The flexibility coefficient matrix [31] of the three-mass-block model is defined as

$$\mathbf{F} = \begin{bmatrix} f_{22} & f_{23} & f_{24} & f_{25} \\ f_{32} & f_{33} & f_{34} & f_{35} \\ f_{42} & f_{43} & f_{44} & f_{45} \\ f_{52} & f_{53} & f_{54} & f_{55} \end{bmatrix},$$

$$= \begin{bmatrix} \frac{4}{3K_1} + \frac{1}{K_B} & \frac{2}{K_1} + \frac{1}{K_B} & \frac{2}{K_1} + \frac{1}{K_B} & \frac{\mu}{K_1} \\ & \frac{4}{K_1} + \frac{4}{3K_2} + \frac{1}{K_B} & \frac{4}{K_1} + \frac{2}{K_2} + \frac{1}{K_B} & \frac{2\mu}{K_1} + \frac{\mu}{K_2} \\ & & \frac{4}{K_1} + \frac{4}{K_2} + \frac{4}{3K_3} + \frac{1}{K_B} & \frac{2\mu}{K_1} + \frac{2\mu}{K_2} + \frac{\mu}{K_3} \\ \textit{symm} & & & \frac{1}{K_1} + \frac{1}{K_2} + \frac{1}{K_3} \end{bmatrix}, \tag{5}$$

where $K_1 = 2\pi aEh/l_1$, $K_2 = 2\pi aEh/l_2$, and $K_3 = 2\pi aEh/l_3$ are the axial rigidities of the tank wall surrounding the mass blocks m_1, m_2, and m_3, respectively; K_B is the rigidity of the tank bottom.

The stiffness coefficient matrix $\boldsymbol{K}$ of the three-mass-block model can then be obtained by solving the inverse of matrix $\boldsymbol{D}$ as

$$\mathbf{K} = \mathbf{D}^{-1}, \quad = \begin{bmatrix} k_{22} & k_{23} & k_{24} & k_{25} \\ k_{32} & k_{33} & k_{34} & k_{35} \\ k_{42} & k_{43} & k_{44} & k_{45} \\ k_{52} & k_{53} & k_{54} & k_{55} \end{bmatrix}. \tag{6}$$

The relationships between the springs in Figure 1(c) and the elements of the stiffness matrix $\mathbf{K}$ are shown in the following equation:

$$\begin{aligned} K_{23} &= -k_{23}; \\ K_{24} &= -k_{24}; \\ K_{25} &= -k_{25}; \\ K_{34} &= -k_{34}; \\ K_{35} &= -k_{35}; \\ K_{45} &= -k_{45}; \\ K_{12} &= k_{22} + k_{23} + k_{24} + k_{25}; \\ K_{13} &= k_{32} + k_{33} + k_{34} + k_{35}; \\ K_{14} &= k_{42} + k_{43} + k_{44} + k_{45}; \\ K_{15} &= k_{52} + k_{53} + k_{54} + k_{55}. \end{aligned} \tag{7}$$

3. Simulation Results

3.1. Model of the Liquid Storage Tank. The structure of the four-stage series liquid storage tank is shown in Figure 2, which is composed of four cylindrical flat bottom tanks I–IV, a connection segment, and a conical head. The bottom of the tank is fixed on the foundation by bolts. The structural dimensions and material properties of the tank are shown in Table 1. The four storage tanks I–IV are filled with a liquid, and the liquid mass in each tank is 35 tons, 45 tons, 25 tons, and 10 tons, respectively.

The mechanical model of the storage tank established by the aforementioned method is shown in Figure 3. According to the geometric attributes of the tank wall and the connection segment, the whole structure is assumed to be a hollow circular beam element with variable thickness and cross section. In the finite element model, the structure of the tank is meshed by the three-dimensional and three-node Timoshenko beam elements. The elastoplastic characteristic of the material is considered. The connecting segments and the tanks are connected by flanges and bolts, and the strength and rigidity of the connecting parts have been predesigned with sufficient margin. The connection segments are also treated as the hollow cylindrical structure, and the thickness is obtained by the stiffness equivalent method. Therefore, the connection segments can also be meshed by the Timoshenko beam elements, and according to its structural characteristics, the mesh of the section is locally refined. The finite element model of the four-stage series liquid storage tank established in ANSYS is shown in Figure 4.

The assignment process of liquid mass effects can be implemented as follows: taking the liquid mass m_{l1} as an example, as illustrated in Figure 1, the horizontal mass effects m_{l1x} and m_{l1z} are equally distributed to the nodes from m_3 to m_i near the liquid; its vertical mass effect m_{l1y} is connected to the liquid mass m_{l2}, m_{l3}, and the related beam nodes through the springs K_{14}, K_{24}, K_{34}, and K_{45}. The spring-mass system is composed of the concentrated mass m_{l1}, m_{l2}, and m_{l3}, and the springs can then be used to simulate the vertical seismic response of the liquid mass in the storage tank.

3.2. Adjustment of the Seismic Wave. Seismic amplitude (or intensity) includes peak acceleration, peak velocity, and peak displacement of the seismic wave. In seismic analysis, the peak value of the acceleration of ground motion is generally used as the strength standard. The selected ground motion record should be adjusted according to an appropriate proportion so that the peak acceleration of the selected wave is equivalent to that of the corresponding seismic fortification intensity. The adjustment formula is

$$a'(t) = \frac{A'_{\max}}{A_{\max}} a(t), \tag{8}$$

where $a'(t)$ and $A'_{\max}$ represent the adjusted seismic acceleration curve and peak value, respectively; $a(t)$ and $A_{\max}$ represent the original recorded seismic acceleration curve and peak value, respectively.

The acceleration curve of the adjusted El Centro earthquake wave with 8° fortification intensity is shown in Figure 5, and its peak acceleration is set to be 0.2 g. The seismic waves along the x-, y-, and z-axis are all used as input excitations, and the peak acceleration ratio among them is set as x: y: $z = 1 : 0.65 : 0.85$.

3.3. Seismic Response Curve of the Top Node. Taking the top node o, as illustrated in Figure 3, of the liquid storage tank as the study object, the curves of displacement and acceleration of this node along the horizontal direction (x-axis and z-axis) and the vertical direction (y-axis) are shown in Figures 6–11, respectively.

It can be seen from Figures 6–8 that, under the action of earthquake excitation, the top node o has endured large vibration displacements. The maximum amplitude along the x-axis is 0.264 m, which occurred at the time $t = 6.5$ s. The vibration displacement along the z-axis is similar to that of the x-axis, but the overall amplitude is slightly smaller, which is due to the fact that the amplitude of seismic acceleration input along the z-axis is smaller than that along the x-axis. The displacement responses in these two directions firstly increase with the increase of the seismic acceleration and then attenuate. In the entire time history, the waves generally present a "spindle" structure with a short front and a long rear, which is caused by the fact that the energy of the seismic wave is mainly concentrated in the early stage. In Figure 7,

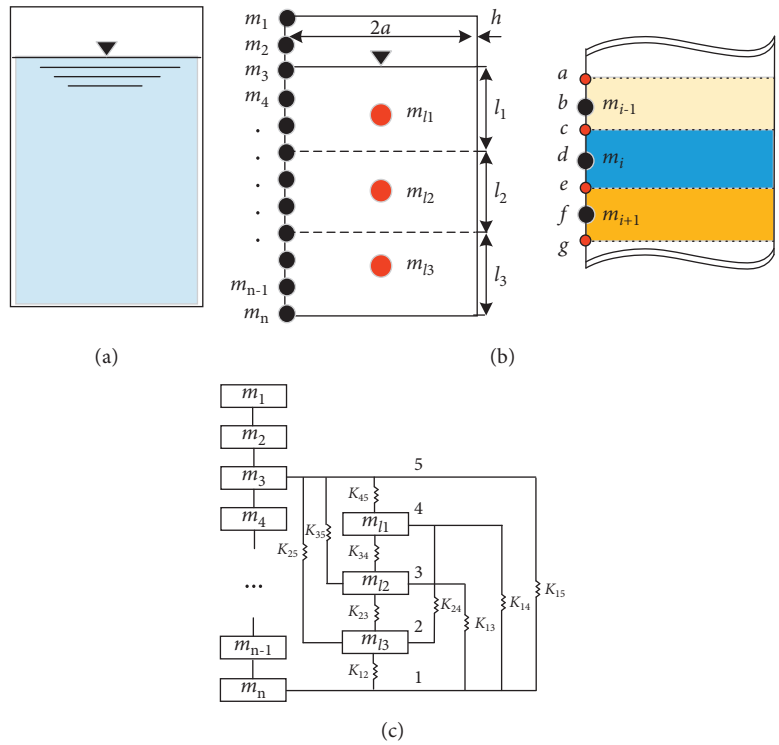

Figure 1: Three-mass-block model of the single-stage liquid storage tank. (a) Structure diagram. (b) Mechanical model. (c) Calculation model.

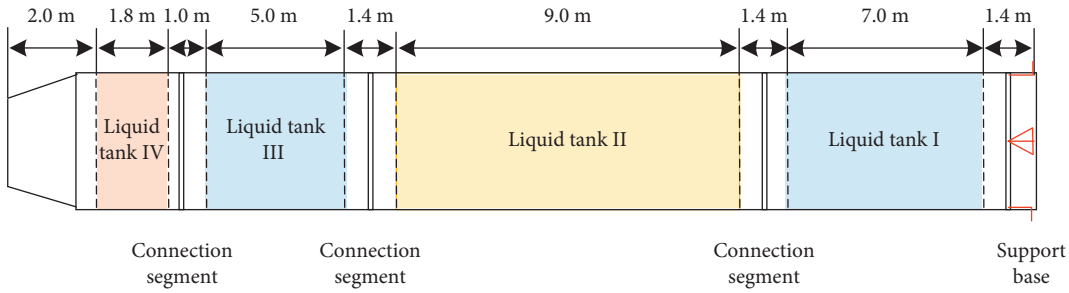

Figure 2: Structure of the four-stage series liquid storage tank.

Table 1: Structural dimensions and material properties of the liquid storage tank.

Parameter	Length (m)	Diameter (m)	Thickness (mm)	Elastic modulus (GPa)	Yield strength (MPa)	Tensile strength (MPa)	Poisson's ratio
Value	30	3.0	3.5	70	300	420	0.33

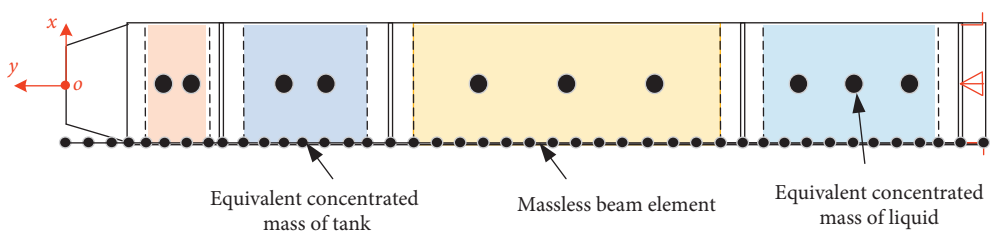

Figure 3: Mechanical model of the liquid storage tank (the springs are omitted).

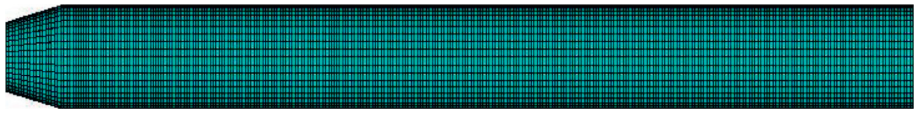

Figure 4: Finite element model of the liquid storage tank.

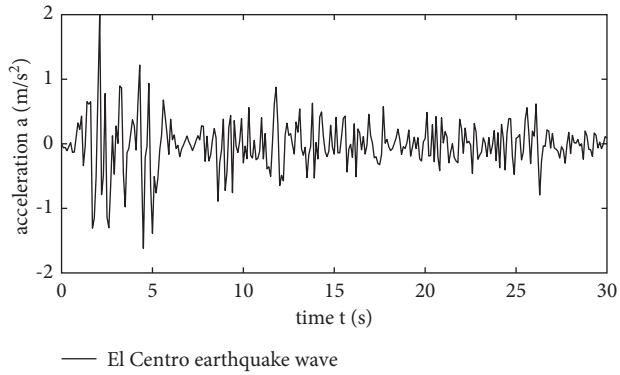

Figure 5: Adjusted El Centro seismic wave with 8° fortification intensity.

due to the large axial stiffness of the storage tank, the vibration displacement of the node along the y-axis is very tiny and within 0.5 mm most of the time. The reason for the notable displacement in the initial stage is that the gravity acceleration is applied to the liquid storage tank in the form of a step function at the initial time of calculation. The notable displacement fluctuation is the step response of the system to the gravity acceleration.

The peak value of the vibration acceleration of the node o along the x-axis is about 3.382 m/s^2, which occurred at time $t = 2.1$ s. It is consistent with the peak time of the input seismic wave, and the amplification factor of peak acceleration of the node along this direction is $\beta_x = 1.691$. The peak value of the vibration acceleration of the node along the z-axis is about 2.875 m/s^2, which also occurred at $t = 2.1$ s. The amplification factor of the peak acceleration of the node along this direction is $\beta_y = 1.438$. Ignoring the step effect of the tank on the gravity acceleration at the initial stage, the longitudinal vibration acceleration of the node caused by the ground motion is relatively small, which is basically within the range of ±0.2 m/s^2. The calculation results show that the seismic wave has a greater impact on the lateral vibration of the tank and less impact on the longitudinal vibration. This is mainly due to that the longitudinal tensile and compression stiffness of the storage tank is much greater than its lateral bending stiffness.

3.4. Vertical Vibration of the Liquid in the Tank. The seismic responses of the acceleration of the liquid mass center in tanks I–IV are shown in Figures 12–15. It can be seen that the liquid has obvious vibration fluctuations along the vertical direction since the influence of the flexibility of the tank on the liquid is considered, as illustrated in Figure 1(c). The acceleration values of the mass center of liquid in tanks I and II are obvious and reach about 0.9 m/s^2. However, the values of the mass center of the liquid in tanks III and IV are neglectable within the range of ±0.2 m/s^2, which is equivalent to the value of the top node o. The differences of the vibration acceleration of the liquid mass center in different tanks can be explained as follows: in equations (5)–(7), the stiffness coefficient matrix K of the three-mass-block model includes the rigidity of the tank wall and the bottom. Compared with the storage tanks III and IV, the lengths of the storage tanks I and II are much longer, as illustrated in Figure 2, which result in the two tanks having lower rigidities. In addition, the liquid mass in the two tanks is much heavier. The lower tank rigidity and heavier liquid mass inevitably cause more significant seismic responses of the liquid in tanks I and II. On the contrary, the lengths of the tanks III and IV are much shorter, which result in the higher rigidities of the two tanks. Moreover, the liquid mass in the tanks is much lighter. Therefore, the higher tank rigidity and lighter liquid mass cause minor seismic responses of the liquid in tanks III and IV.

3.5. Diagram of Combined Deformation-Axial Coordinate (the Moment of Maximum Deformation). It can be seen from Figures 6 and 8 that the maximum deformation of the whole structure of the tank occurred at the time $t = 6.5$ s. At this moment, the combined deformation curve of the nodes along the axial direction of the tank is shown in Figure 16. The combined deformation of the tank increases with the height of its body. The overall deformation of the tank presents the deformation characteristic of a vertical cantilever beam subjected to a horizontal load. The maximum combined deformation of the tank is 0.331 m at the coordinate $y = 0$.

3.6. Time History Curve of Stress at the Supporting Point of the Tank. The time history curve of the stress of the grid point, where the supporting point of the tank is located, on the beam element is shown in Figure 17. The maximum stress is

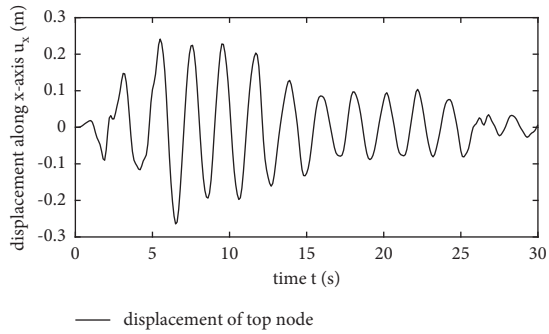

Figure 6: Displacement of top node (o) along the (x)-axis.

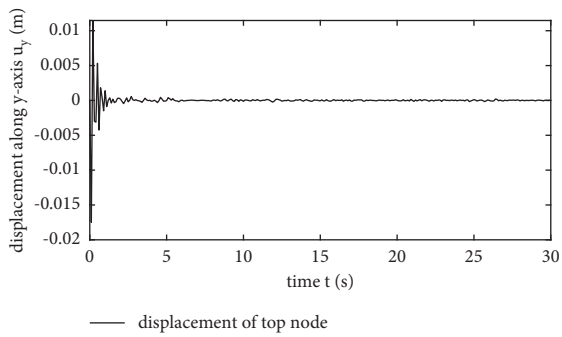

Figure 7: Displacement of top node (o) along the (y)-axis.

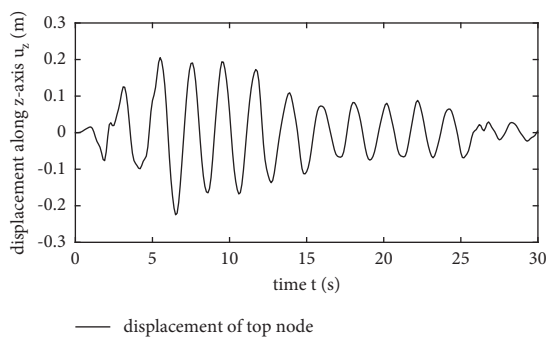

Figure 8: Displacement of top node (o) along the (z)-axis.

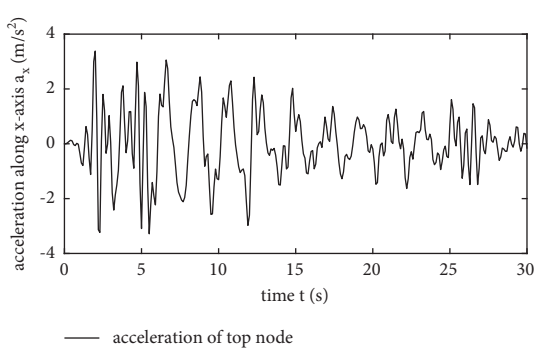

Figure 9: Acceleration of top node (o) along the (x)-axis.

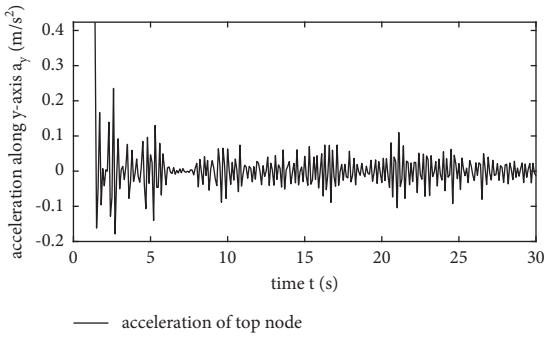

Figure 10: Acceleration of top node (o) along the (y)-axis with ignoring the step effect of gravitational acceleration at the initial moment.

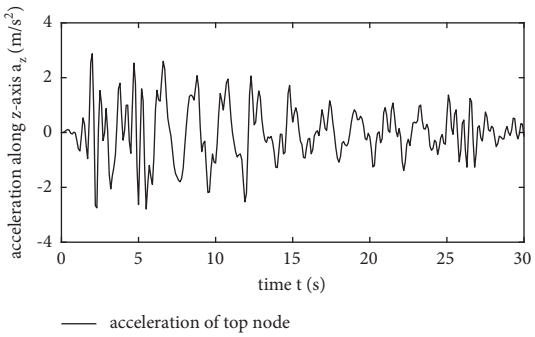

Figure 11: Acceleration of top node (o) along the (z)-axis.

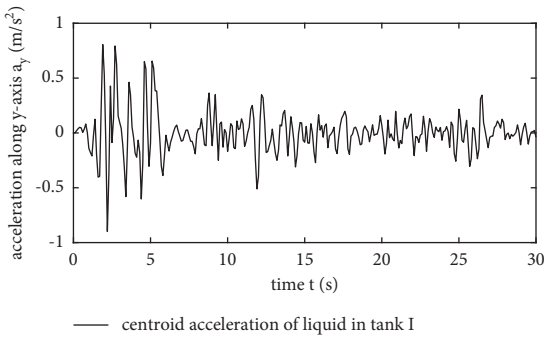

Figure 12: Acceleration curve of mass center of the liquid in tank I.

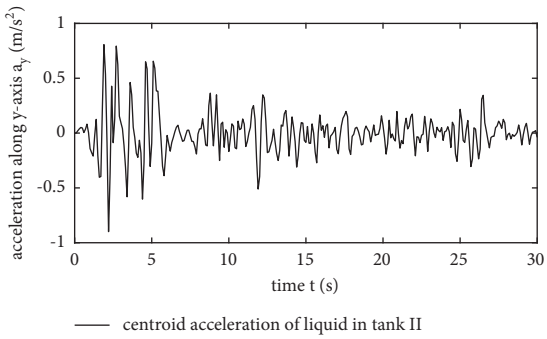

Figure 13: Acceleration curve of mass center of the liquid in tank II.

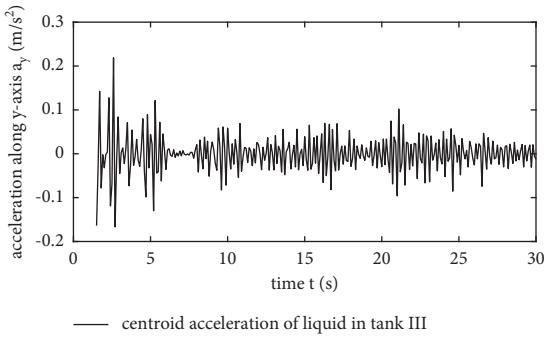

Figure 14: Acceleration curve of mass center of the liquid in tank III.

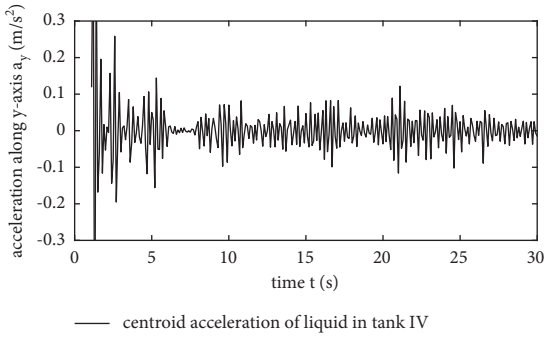

Figure 15: Acceleration curve of mass center of the liquid in tank IV.

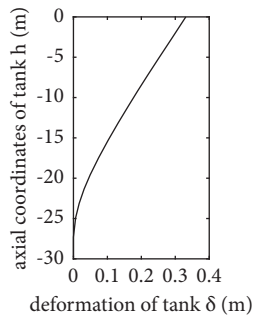

Figure 16: Diagram of the combined deformation-axial coordinate (the moment of maximum deformation).

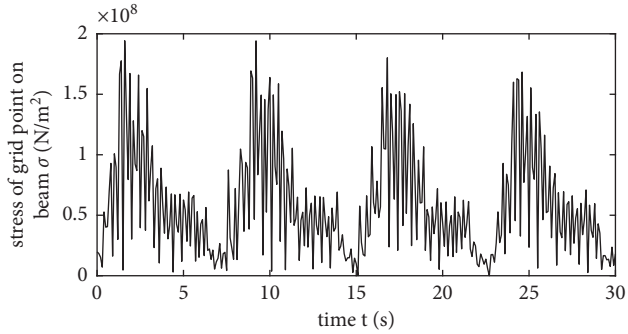

Figure 17: Time history curve of stress of the supporting point.

Figure 18: The scaled-down model of the four-stage storage tank.

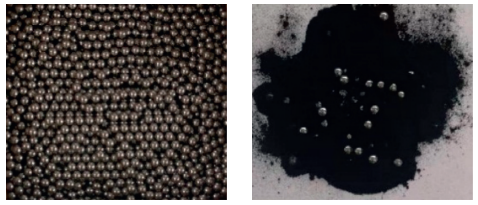

(a) (b)

Figure 19: Equivalent filling material for liquid. (a) Lead balls. (b) Mixture of lead balls and iron powder.

(a) (b)

Figure 20: Layout of measuring sensors. (a) Measuring position of the acceleration sensor. (b) Measuring position of the strain gauge (a pair of strain gauges in a T-shaped arrangement).

194.24 MPa, which is less than the yield stress of the material. The stress curve presents the characteristic of periodic fluctuations, and the overall trend of the attenuation is consistent with the decrease of the input intensity of the seismic wave.

4. Test Verification

A scaled-down test model of the four-stage series storage tank, as shown in Figure 18, is manufactured to verify the accuracy of the research model presented in this paper. The scaled model is mainly composed of the conical top, four-stage storage tanks I–IV, and end support. Different sections of the test model are connected by flanges and bolts. In order to simulate the coupling effect of the liquid in the tank, lead balls and a mixture of lead balls and iron powder, as shown in Figure 19, are filled in different tanks. Tanks II and IV are filled with lead balls, and tanks I and III are filled with a mixture of lead balls and iron powder. The experiment was carried out on the earthquake occurrence test bed of

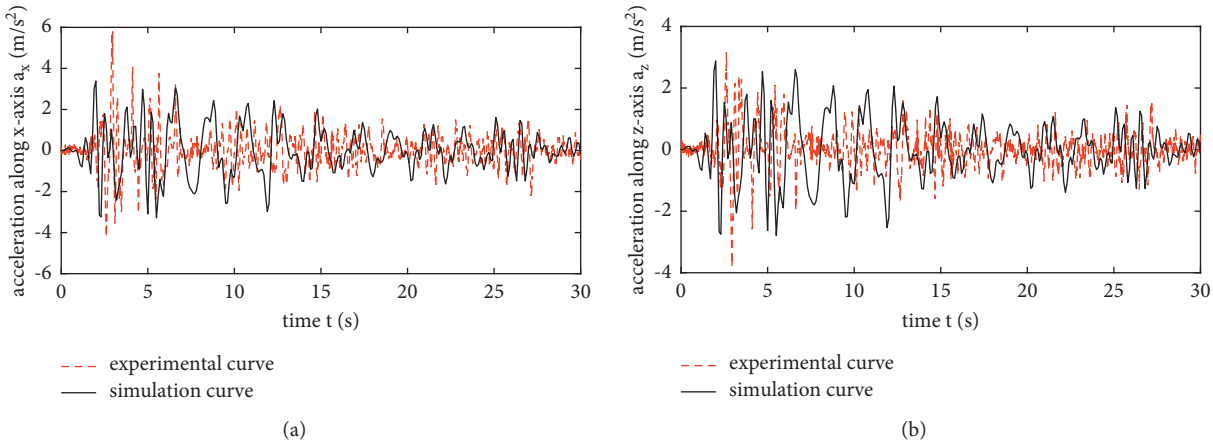

Figure 21: Comparison of lateral acceleration results of the top node. (a) Acceleration curve along the (x)-axis. (b) Acceleration curve along the (z)-axis.

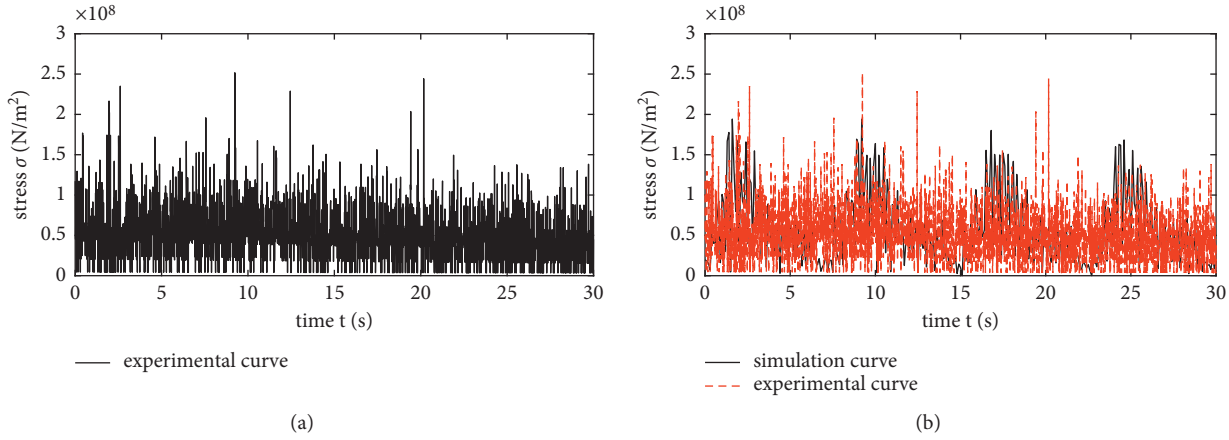

Figure 22: Comparison of stress results of supporting point. (a) Test result curve. (b) Comparison curves between the test model and calculation model.

Lanzhou University of Technology. The measuring positions of the acceleration sensor and the strain gauge are shown in Figure 20.

4.1. Comparison of Acceleration Results. The comparisons between the test curve and the calculated curve of acceleration of the top node o along the x-axis and the z-axis are shown in Figure 21. It can be seen that the two curves are in good agreement with the trend of the waveform amplitude. However, the oscillating periods of them are significantly different. The main reason for this can be analyzed as follows: (1) In the numerical model, the frequency of the input seismic wave is set lower ($f = 10$ Hz) to reduce the calculation cost, while in the test model, the frequency is set much higher ($f = 50$ Hz). The differences in the input frequency of seismic excitation lead to the forced vibration frequency of the test model being much greater than that of the calculation model. (2) Due to the limitation of machining technology, the rigidity of the scaled model is greater than that of the calculation model, which leads to the higher natural frequencies and response frequencies in the test model.

4.2. Comparison of Stress Results. The time history curve of the stress of the supporting part on the test model is shown in Figure 22(a), and the comparison between the test curve and the calculated curve is shown in Figure 22(b). It can be seen that the two curves have similar attenuation and periodic characteristics, and the amplitudes of them are also in good agreement. Compared with the stress curve of the calculation model, the curve of the test model has more peak burrs, which is mainly caused by the interference of external signals on the sensors.

5. Conclusions

The seismic response of the multistage series liquid storage tank was simulated and verified in this paper. The structural flexibility of the tank and the liquid-structure coupling characteristics between the tank wall and the liquid were considered

in the study. The additional mass matrix representing the effect of the liquid on the structure was obtained by assuming that the liquid is incompressible and inviscid and has irrotational motion. In order to simulate the longitudinal vibration characteristics of the liquid storage tank, a multimass-block and spring model was employed to equivalent the longitudinal vibration of the liquid. The relationships between the connection springs and the elements of the stiffness matrix of the spring-mass model were explicitly deduced.

The seismic response analysis of the four-stage series liquid tank was carried out in ANSYS. The acceleration, deformation, and stress responses of the tank were obtained. In addition, because the influence of the flexibility of the tank wall on the longitudinal vibration of the liquid was considered in the model, the vertical vibrations of the liquid were also obtained. A scaled-down model of the four-stage series storage tank was processed and manufactured, and the seismic test was subsequently carried out. The experimental results are in good agreement with the simulation results, which verified the effectiveness of the modeling method in this paper.

Data Availability

The data used to support the findings of this study are available from the corresponding author upon request.

Conflicts of Interest

The authors declare no potential conflicts of interest with respect to the research, authorship, and/or publication of this article.

Acknowledgments

The authors wish to express their sincere thanks to the sponsors and to the reviewers for useful and important comments. This research was financially supported by the National Natural Science Foundation of China (Grant no. 51505485), the Basic Research Program of Natural Science in Shaanxi Province (Grant no. 2020JM-640), the Special Item Funds for High-level Personnel of Xijing University (Grant no. XJ18B08), and the Youth Innovation Team of Shaanxi Universities.

References

[1] M. K. Shrimali and R. S. Jangid, "Seismic analysis of base-isolated liquid storage tanks," *Journal of Sound and Vibration*, vol. 275, no. 1-2, pp. 59–75, 2004.

[2] X. Meng, X. Li, X. Xu, J. Zhang, W. Zhou, and D. Zhou, "Earthquake response of cylindrical storage tanks on an elastic soil," *Journal of Vibration Engineering & Technologies*, vol. 7, no. 5, pp. 433–444, 2019.

[3] M. Bovo, A. Barbaresi, and D. Torreggiani, "Definition of seismic performances and fragility curves of unanchored cylindrical steel legged tanks used in wine making and storage," *Bulletin of Earthquake Engineering*, vol. 18, no. 8, pp. 3711–3745, 2020.

[4] C.-C. Yu and A. S. Whittaker, "Review of analytical studies on seismic fluid-structure interaction of base-supported cylindrical tanks," *Engineering Structures*, vol. 233, Article ID 111589, 2021.

[5] G. W. Housner, "The dynamic behavior of water tanks," *Bulletin of the Seismological Society of America*, vol. 53, no. 2, pp. 381–387, 1963.

[6] E. Rosenblueth and N. M. Newmark, *Fundamentals of Earthquake Engineering*, Prentice-Hall, Englewood Cliffs, NJ, USA, 1971.

[7] M. A. Haroun, "Vibration studies and tests of liquid storage tanks," *Earthquake Engineering & Structural Dynamics*, vol. 11, no. 2, pp. 179–206, 1983.

[8] A. Fiore, C. Rago, I. Vanzi, R. Greco, and B. Briseghella, "Seismic behavior of a low-rise horizontal cylindrical tank," *International Journal of Advanced Structural Engineering*, vol. 10, no. 2, pp. 143–152, 2018.

[9] D. K. Fotini and G. D. Hatzigeorgiou, "Water and wastewater steel tanks under multiple earthquakes," *Soil Dynamics and Earthquake Engineering*, vol. 100, pp. 445–453, 2017.

[10] G. W. Housner, "Earthquake pressures on fluid containers, eighth technical report under office of naval research," California Institute of Technology, Pasadena, CA, USA, Project Designation No. 081-095, 1954.

[11] G. W. Housner, "Dynamic pressures on accelerated fluid containers," *Bulletin of the Seismological Society of America*, vol. 47, pp. 313–346, 1957.

[12] A. Rawat, V. Matsagar, and A. K. Nagpal, "Coupled acoustic-structure interaction in cylindrical liquid storage tank subjected to bi-directional excitation," in *Advances in Structural Engineering*, Springer, New Delhi, India, 2015.

[13] M. K. Shrimali and R. S. Jangid, "Earthquake response of isolated elevated liquid storage steel tanks," *Journal of Constructional Steel Research*, vol. 59, no. 10, pp. 1267–1288, 2003.

[14] O. Curadelli, "Equivalent linear stochastic seismic analysis of cylindrical base-isolated liquid storage tanks," *Journal of Constructional Steel Research*, vol. 83, pp. 166–176, 2013.

[15] S. K. Saha, V. A. Matsagar, and A. K. Jain, "Seismic fragility of base-isolated water storage tanks under non-stationary earthquakes," *Bulletin of Earthquake Engineering*, vol. 14, no. 4, pp. 1153–1175, 2016.

[16] A. S. Ayman and M. El-Sharkawy, "Seismic response of base isolated liquid storage ground tanks," *Ain Shams Engineering Journal*, vol. 2, pp. 33–42, 2011.

[17] L. Yuan, J. Sun, and Z. Sun, "Simplified mechanical model for seismic design of horizontal storage tank considering soil-tank-liquid interaction," *Ocean Engineering*, vol. 198, Article ID 106953, 2020.

[18] V. R. Panchal and R. S. Jangid, "Variable friction pendulum system for seismic isolation of liquid storage tanks," *Nuclear Engineering and Design*, vol. 238, no. 6, pp. 1304–1315, 2008.

[19] V. Ozsarac, E. Brunesi, and R. Nascimbene, "Earthquake-induced nonlinear sloshing response of above-ground steel tanks with damped or undamped floating roof," *Soil Dynamics and Earthquake Engineering*, vol. 144, Article ID 106673, 2021.

[20] S. A. Karamanos, "Sloshing effects on the seismic design of horizontal-cylindrical and spherical vessels," in *Proceedings of the 2004 ASME Pressure Vessels and Piping Division Conference*, San Diego, CA, USA, July 2004.

[21] M. A. Platyrrachos and S. A. Karamanos, "Finite element analysis of sloshing in horizontal-cylindrical industrial vessels under earthquake loading," in *Proceedings of the 2005 ASME Pressure Vessels and Piping Division Conference*, Denver, CO, USA, July 2005.

[22] L. A. Patkas and S. A. Karamanos, "Variational analysis of sloshing in spherical industrial vessels under earthquake loading," in *Proceedings of the 2006 ASME Pressure Vessels and Piping Division Conference*, Vancouver, Canada, July 2006.

[23] J. Li, X. You, H. Cui, Q. He, and J. Ju, "Analysis of large concrete storage tank under seismic response," *Journal of Mechanical Science and Technology*, vol. 29, no. 1, pp. 85–91, 2015.

[24] A. Rawat, V. Mittal, T. Chakraborty, and V. Matsagar, "Earthquake induced sloshing and hydrodynamic pressures in rigid liquid storage tanks analyzed by coupled acoustic-structural and Euler-Lagrange methods," *Thin-Walled Structures*, vol. 134, pp. 333–346, 2019.

[25] A. Rawat, V. A. Matsagar, and A. K. Nagpal, "Numerical study of base-isolated cylindrical liquid storage tanks using coupled acoustic-structural approach," *Soil Dynamics and Earthquake Engineering*, vol. 119, pp. 196–219, 2019.

[26] M. R. Shekari, N. Khaji, and M. T. Ahmadi, "On the seismic behavior of cylindrical base-isolated liquid storage tanks excited by long-period ground motions," *Soil Dynamics and Earthquake Engineering*, vol. 30, no. 10, pp. 968–980, 2010.

[27] J. C. Drosos, S. V. Tsinopoulos, and D. L. Karabalis, "Seismic retrofit of spherical liquid storage tanks with energy dissipative devices," *Soil Dynamics and Earthquake Engineering*, vol. 119, pp. 158–169, 2019.

[28] E. María and O. Curadelli, "Experimental and numerical study of the response of cylindrical steel tanks under seismic excitation," *International Journal of Civil Engineering*, vol. 16, pp. 793–805, 2018.

[29] J. H. Park, D. Bae, and C. K. Oh, "Experimental study on the dynamic behavior of a cylindrical liquid storage tank subjected to seismic excitation," *International Journal of Steel Structures*, vol. 16, no. 3, pp. 935–945, 2016.

[30] D. Bae and J. Ho Park, "Shaking table test of steel cylindrical liquid storage tank considering the roof characteristics," *International Journal of Steel Structures*, vol. 18, no. 4, pp. 1167–1176, 2018.

[31] D. Wenbin and Y. Tang, "Study on application of dynamical models for the longitudinal vibration of liquid-propellant launch vehicles," *Structure & Environment Engineering*, vol. 42, no. 6, pp. 1–10, 2015.